

ozone loss due to denitrification is limited to below ~30% [i.e., 0.7 ppmv additional loss divided by (1.7 + 0.7) ppmv total loss for the 2010 decade].

The prospect of widespread Arctic denitrification in the future is real even if lower stratospheric temperatures are cooling at a rate of only 1 K per decade. The development of a persistently cold and stable vortex is not required for Arctic denitrification to occur. For Arctic denitrification to be initiated, longer PSC lifetimes, similar to those of the Antarctic during mid to late June, need to be maintained only for periods less than 2 weeks. Widespread severe denitrification could enhance future Arctic ozone loss by up to 30%. Overall, though, the role of denitrification in the depletion of Arctic ozone in large-scale models is still uncertain, and the effect of changes in temperature and water vapor on denitrification needs to be quantified to better understand and predict Arctic ozone trends.

References and Notes

1. S. Solomon, *Rev. Geophys.* **37**, 275 (1999).
2. *WMO Scientific Assessment of Ozone Depletion: 1998, Rep. 44* (1999).
3. O. B. Toon, P. Hamill, R. P. Turco, J. Pinto, *Geophys. Res. Lett.* **13**, 1284 (1986).
4. P. J. Crutzen and F. Arnold, *Nature* **324**, 651 (1986).
5. R. J. Salawitch, G. P. Gobbi, S. C. Wofsy, M. B. McElroy, *Nature* **339**, 525 (1989).
6. R. S. Stolarski, *Nature* **389**, 788 (1997).
7. W. H. Brune *et al.*, *Science* **252**, 1260 (1991).
8. W. H. Brune, D. W. Toohey, J. G. Anderson, K. R. Chan, *Geophys. Res. Lett.* **17**, 505 (1990).
9. C. R. Webster *et al.*, *Science* **261**, 1130 (1993).
10. D. W. Toohey *et al.*, *Science* **261**, 1134 (1993).
11. M. L. Santee *et al.*, *Science* **267**, 849 (1995).
12. J. W. Waters *et al.*, *Nature* **362**, 597 (1993).
13. D. G. Andrews, *Pure Appl. Geophys.* **130**, 213 (1989).
14. D. W. Waugh and W. J. Randel, *J. Atmos. Sci.* **56**, 1594 (1999).
15. M. Rex *et al.*, *Nature* **389**, 835 (1997).
16. N. Larsen *et al.*, *Geophys. Res. Lett.* **21**, 1611 (1994).
17. G. L. Manney *et al.*, *Nature* **370**, 429 (1994).
18. G. L. Manney, *Geophys. Res. Lett.* **23**, 85 (1996).
19. *et al.*, *Geophys. Res. Lett.* **24**, 2697 (1997).
20. G. L. Manney *et al.*, *J. Atmos. Sci.* **52**, 3069 (1995).
21. M. P. Chipperfield and R. L. Jones, *Nature* **400**, 551 (1999).
22. M. L. Santee, G. L. Manney, L. Froidevaux, W. G. Read, J. Waters, *J. Geophys. Res.* **104**, 8225 (1999).
23. A. E. Dessler, J. Wu, M. L. Santee, M. R. Schoeberl, *J. Geophys. Res.* **104**, 13993 (1999).
24. A. E. Roche *et al.*, *J. Atmos. Sci.* **51**, 2877 (1994).
25. A. E. Waibel *et al.*, *Science* **283**, 2064 (1999).
26. D. W. Waugh, *J. Geophys. Res.* **102**, 13119 (1997).
27. H. A. Michelsen, G. L. Manney, M. R. Gunson, R. Zander, *J. Geophys. Res.* **103**, 28347 (1998).
28. Y. Kondo *et al.*, *J. Geophys. Res.* **104**, 8215 (1999).
29. G. L. Manney *et al.*, *J. Geophys. Res.* **104**, 18841 (1999).
30. M. Rex *et al.*, *J. Geophys. Res.* **104**, 26611 (1999).
31. R. A. Plumb, D. W. Waugh, M. P. Chipperfield, *J. Geophys. Res.* **105**, 10062 (2000).
32. D. W. Fahey *et al.*, *Nature* **344**, 321 (1990).
33. S. R. Kawa *et al.*, *J. Geophys. Res.* **97**, 7925 (1992).
34. H. Fischer *et al.*, *J. Geophys. Res.* **102**, 23559 (1997).
35. H. F. Schlager and F. Arnold, *Geophys. Res. Lett.* **17**, 433 (1990).
36. F. Arnold, V. Buger, K. Gollinger, M. Roncossek, *J. Atmos. Chem.* **30**, 49 (1998).
37. K. S. Carslaw *et al.*, *J. Geophys. Res.* **103**, 5785 (1998).
38. H. Vomel, S. J. Oltmans, D. J. Hofmann, T. Deshler, J. M. Rosen, *J. Geophys. Res.* **100**, 13919 (1995).

39. K. S. Carslaw *et al.*, *Nature* **391**, 675 (1998).
40. M. L. Santee *et al.*, *J. Geophys. Res.* **103**, 13285 (1998).
41. H. C. Pumphrey, *J. Geophys. Res.* **104**, 9399 (1999).
42. J. L. Mergenthaler, J. B. Kumer, A. E. Roche, S. T. Massie, *J. Geophys. Res.* **102**, 19161 (1997).
43. A. Tabazadeh, R. P. Turco, K. Drdla, M. Z. Jacobson, O. B. Toon, *Geophys. Res. Lett.* **21**, 1619 (1994).
44. M. R. Schoeberl *et al.*, *J. Geophys. Res.* **97**, 7859 (1992).
45. D. J. Hofmann and T. Deshler, *J. Geophys. Res.* **96**, 2897 (1991).
46. T. Deshler, A. Adriani, D. J. Hofmann, G. P. Gobbi, *Geophys. Res. Lett.* **18**, 1999 (1991).
47. H. A. Chang, T. Koop, L. T. Molina, M. J. Molina, *J. Phys. Chem.* **103**, 2673 (1999).
48. A. Tabazadeh, S. T. Martin, J. S. Lin, *Geophys. Res. Lett.* **27**, 1111 (2000).
49. S. Pawson and B. Naujokat, *Geophys. Res. Lett.* **24**, 575 (1997).
50. V. Ramaswamy, M. D. Schwartzkopf, W. Randel, *Nature* **382**, 616 (1996).
51. D. T. Shindell, D. Rind, P. Lonergan, *Nature* **392**, 589 (1998).
52. S. J. Oltmans and D. J. Hofmann, *Nature* **374**, 146 (1995).
53. G. E. Nedoluha *et al.*, *J. Geophys. Res.* **103**, 3531 (1998).

54. S. J. Evans, R. Toumi, J. E. Harries, M. P. Chipperfield, J. M. Russell III, *J. Geophys. Res.* **103**, 8715 (1998).
55. P. M. de F. Forster and K. P. Shine, *Geophys. Res. Lett.* **26**, 3309 (1999).
56. M. Y. Danilin, N. D. Sze, M. K. W. Ko, J. M. Rodriguez, A. Tabazadeh, *Geophys. Res. Lett.* **25**, 2141 (1998).
57. M. Y. Danilin, N. D. Sze, M. K. W. Ko, J. M. Rodriguez, M. J. Prather, *Geophys. Res. Lett.* **23**, 153 (1996).
58. G. P. Brasseur, X. Tie, P. J. Rasch, F. Lefevre, *J. Geophys. Res.* **102**, 8909 (1997).
59. R. W. Portmann *et al.*, *J. Geophys. Res.* **101**, 22991 (1996).
60. M. P. Chipperfield and J. A. Pyle, *J. Geophys. Res.* **103**, 28389 (1998).
61. We thank G. Manney, D. Kinnison, M. Tolbert, and K. Drdla for helpful comments and suggestions. Supported by NASA's Upper Atmosphere Research Satellite (UARS) program and a Presidential Early Career Award for Scientists and Engineers (A.T.). The work at the Jet Propulsion Laboratory was done under contract with NASA. M.Y.D. is supported by NASA Atmospheric Chemistry Modeling and Analysis Program (ACMAP) and UARS guest investigator programs. H.C.P. was supported by UK Natural Environment Research Council grant GR3/10111.

15 November 1999; accepted 12 April 2000

Field Measurement of Slow Metamorphic Reaction Rates at Temperatures of 500° to 600°C

Ethan F. Baxter* and Donald J. DePaolo

High-temperature metamorphic reaction rates were measured using strontium isotopic ratios of garnet and whole rock from a field site near Simplon Pass, Switzerland. For metamorphic conditions of cooling from 612° ± 17°C to 505° ± 15°C at pressures up to 9.1 kilobars, the inferred bulk fluid-rock exchange rate is 1.3^{+1.1}_{-0.4} × 10⁻⁷ grams of solid reacted per gram of solid per year, several orders of magnitude lower than laboratory-based estimates. The inferred reaction rate suggests that mineral chemistry may lag the evolving conditions in Earth's crust during mountain building.

Chemical and isotopic compositions of metamorphic minerals are used to determine the history of pressure, temperature, and chemical (P-T-X) evolution in Earth's crust during mountain building. Data interpretation is based on the assumption of local equilibrium (1), which requires that reactions proceed rapidly relative to rates of local P-T-X change. Whether this assumption is warranted is difficult to ascertain. Extrapolation of existing laboratory-based kinetic data (2–5) to natural systems is subject to large uncertainties because the reaction mechanisms (4) and controlling parameters (e.g., departure from equilibrium and reactive surface area) are unknown. There is growing recognition of natural effects attributable to slower reaction rates

(6, 7), but no direct determinations of regional metamorphic reaction rates have been made.

Here, Sr isotopic measurements in metamorphic rocks are used in conjunction with geochronology and numerical models to estimate natural rates of chemical exchange between minerals and intergranular fluid [more generally, the intergranular transporting medium or ITM (8)]. The approach focuses on analysis of isotopic variations along a transect normal to a lithologic contact where there was, before metamorphism, a sharp, step-like contrast in isotopic ratios. During metamorphism, the isotope ratio (⁸⁷Sr/⁸⁶Sr) profile across the contact changes in different ways depending on the relative rates of cross-contact intergranular transport and local solid-ITM exchange (7). Local chemical reactions are mediated by the ITM as solid dissolves and reprecipitates. The isotope ratio is a passive tracer of the bulk solid reactivity. The driving potential for the bulk solid reaction is

Department of Geology and Geophysics, University of California, 301 McCone Hall, Berkeley, CA 94720, USA.

*To whom correspondence should be addressed. E-mail: ebaxter@uclink4.berkeley.edu

REPORTS

the overall chemical affinity (9), which is determined by changes in the P-T-X state of the system.

Transport normal to the contact occurs by diffusion through the ITM (10). The ability of the bulk solid to exchange Sr and maintain chemical equilibrium with the changing ITM depends on the bulk reaction rate, R [see (11) for definition], and the effective diffusivity, D^* , of Sr in the ITM. This balance can be expressed in terms of Le_{Sr} , the diffusive equilibration length (12):

$$Le_{Sr} = (D_{Sr}^*/R)^{1/2} \quad (1)$$

where

$$D_{Sr}^* = D_{Sr}\tau/MK_{Sr} \quad (2)$$

and D_{Sr} is the diffusivity of Sr in the ITM, τ is tortuosity, $M = \rho_s(1 - \phi)/(\rho_f\phi)$ (the mass ratio of solid to fluid, where ρ is density and ϕ is porosity), and K_{Sr} is the equilibrium solid-fluid distribution coefficient.

The following equations (7, 13) are used to model the evolution of the $^{87}Sr/^{86}Sr$ ratio in the ITM (r_f) and the solid (r_s):

$$\partial r_s/\partial t = -R(r_s - r_f) + \lambda r_{ps} \quad (3)$$

$$\begin{aligned} \partial r_f/\partial t = & MK_{Sr}D_{Sr}^*(\partial^2 r_f/\partial x^2) \\ & + RMK_{Sr}(r_s - r_f) + \lambda r_{ps} \end{aligned} \quad (4)$$

where x is the spatial coordinate and λr_{ps} (14) accounts for the radioactive decay of ^{87}Rb to ^{87}Sr . Analytical solutions and modeling show that changes only in MK do not affect system behavior (7). The adjustable parameters are R and D_{Sr}^* . The pattern of isotopic ratios in the rocks and minerals about the contact allows us to constrain the value of Le_{Sr} and the

integrated amount of reaction over time t :

$$\langle Rt \rangle = \int_{t_{init}}^{t_{final}} R(\tau)d\tau \quad (5)$$

Independent geochronology allows us to constrain absolute values for t_{init} , t_{final} , D_{Sr}^* , and R .

A unique aspect of our approach is the use of garnet porphyroblasts. Although whole-rock measurements yield the final isotopic profile after metamorphic exchange ceases, garnet porphyroblasts preserve a record of the ITM isotopic profile at the time of garnet growth (15). Garnets provide an initial syn-metamorphic condition and time, a constraint that a purely whole-rock study lacks. We know that the bulk solid isotopic profile must have either matched or lagged the ITM (garnet) profile at that time, because the solid $^{87}Sr/^{86}Sr$ changes only by exchanging with the ITM. Subsequent differences between whole-rock and garnet Sr isotopic ratios must have been generated between the time of garnet growth and the cessation of metamorphic exchange, which eliminates the possibility of confusing earlier, diagenetic exchange with metamorphic processes (16).

The field site is located south of Simplon Pass, Switzerland, about 100 m west of Alte Kaserne. It is situated structurally in the Lebendun Nappe on the west flank of the Lepontine Dome (17). Geothermobarometry shows garnet growth conditions to be $\sim 612^\circ \pm 17^\circ C$ and 9.1 ± 0.5 kbar (18). Published garnet ages from the western Lepontine Alps bracket the age of garnet growth to 29.7 ± 4.2 Ma (million years ago) (19). Plagioclase-whole rock Rb-Sr ages show cooling through $\sim 505^\circ \pm 15^\circ C$ at 16.5 ± 1.7 Ma (18).

The measured $^{87}Sr/^{86}Sr$ (18) variation in the amphibolite suggests diffusive exchange with the pelite (Fig. 1). The difference between the garnet and whole-rock profiles indicates that the bulk solid matrix $^{87}Sr/^{86}Sr$ changed after garnet growth as a result of continuing reactive transport (in addition to radioactive decay). Nd isotope data (18) in the amphibolite are constant right up to the contact (20), confirming an original step-like contact.

The time of garnet growth, 29.7 ± 4.2 Ma, is used as the starting point for numerical simulations, t_{init} . Quasi-steady-state ITM and solid profiles for initial ($t_{init} = 29.7$ Ma) values of R and D_{Sr}^* were generated to fit the garnet data (Fig. 1). Numerous model iterations showed that observed garnet (at t_{init}) and whole-rock (at t_{final}) data cannot be reproduced unless the solid already lags the ITM profile at the time of garnet growth.

The plagioclase-whole rock Rb/Sr age of 16.5 ± 1.7 Ma, reflecting the time at which plagioclase closed to further Sr exchange, is taken to represent the end of metamorphic exchange, t_{final} , as plagioclase is the major Sr-bearing phase in the system. This time also corresponds to the onset of rapid exhumation and cooling of the nappe stack (21).

Sensitivity tests using both constant and time-varying values for R and D_{Sr}^* were conducted (Fig. 2). The best fit is obtained for constant R , with $\langle Rt \rangle = 1.75$, and Le_{Sr} increasing from 13 cm at garnet growth conditions to 130 cm at the cessation of metamorphic exchange. Using the geochronological constraints, $R = 1.3 \times 10^{-7} \text{ g g}^{-1} \text{ year}^{-1}$ with D_{Sr}^* increasing log-linearly from 2.0×10^{-9} to $2.0 \times 10^{-7} \text{ m}^2 \text{ year}^{-1}$ (Fig. 2). D_{Sr}^* might increase at lower temperature with increased propensity for brittle fracture during exhumation. The time-integrated

Fig. 1. Whole-rock and garnet Sr isotope data (at 16.5 Ma and 29.7 Ma, respectively) at the study site; 2σ errors are <0.00004 for whole-rock and <0.00009 for garnet. Note the initial, $t_{init} = 29.7 \pm 4.2$ Ma, steady-state solid (solid line) and fluid (dotted line) conditions used for modeling for the best-fit parameters: $R = 1.3 \times 10^{-7} \text{ g g}^{-1} \text{ year}^{-1}$ and $D_{Sr}^*(init) = 2.0 \times 10^{-9} \text{ m}^2 \text{ year}^{-1}$. To get the initial profiles, we estimated the premetamorphic $^{87}Sr/^{86}Sr$ in the amphibolite at 0.7059, the lowest value of garnet far from the contact (5.4 m), and set the premetamorphic pelite $^{87}Sr/^{86}Sr$ to 0.7197 in order to reproduce the inflection point. An evolved steady-state fluid profile was then fit to the garnet data. The corresponding steady-state solid profile follows, and depends on the initial values of R and D_{Sr}^* . Also shown is the lowest value of solid in the amphibolite far from the contact (6.4 m). The garnet at -0.15 m may have lower $^{87}Sr/^{86}Sr$ because of the fine grain size (100 to 150 μm) and lack of zoning, which suggests that this garnet may not have been closed to further exchange after growth.

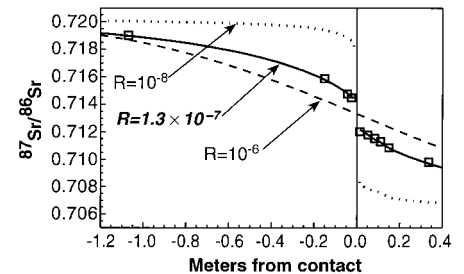
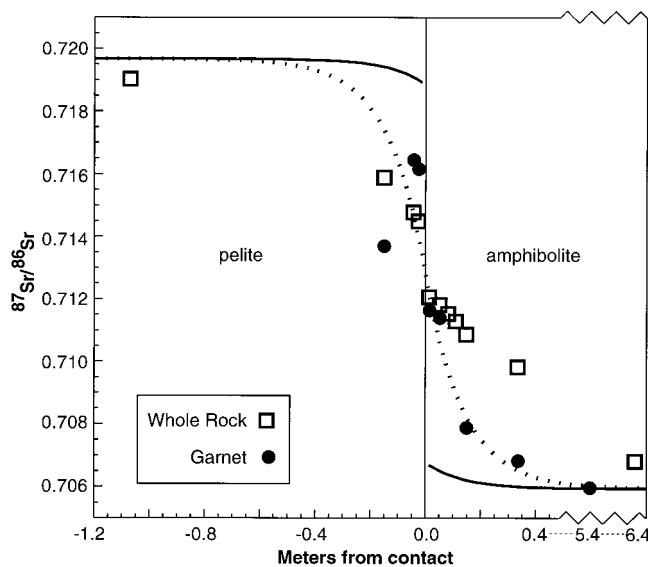


Fig. 2. Calculated model profiles of $^{87}Sr/^{86}Sr$ showing the sensitivity to changes in R . Open squares are the measured whole-rock data at 16.5 Ma. In each case D_{Sr}^* was adjusted to preserve the steady-state match to the garnet data at the start of simulation. For $R = 10^{-8} \text{ g g}^{-1} \text{ year}^{-1}$, $D_{Sr}^*(init) = 1.6 \times 10^{-10}$ and $D_{Sr}^*(final) = 5.0 \times 10^{-7} \text{ m}^2 \text{ year}^{-1}$; for $R = 10^{-6} \text{ g g}^{-1} \text{ year}^{-1}$, $D_{Sr}^*(init) = 1.6 \times 10^{-8}$ and $D_{Sr}^*(final) = 5.4 \times 10^{-8} \text{ m}^2 \text{ year}^{-1}$; and for the best fit, $R = 1.3 \times 10^{-7} \text{ g g}^{-1} \text{ year}^{-1}$, $D_{Sr}^*(init) = 2.0 \times 10^{-9}$ and $D_{Sr}^*(final) = 2.0 \times 10^{-7} \text{ m}^2 \text{ year}^{-1}$. The size of the isotopic step at the contact indicates that R must be $\sim 10^{-7} \text{ g g}^{-1} \text{ year}^{-1}$.

REPORTS

reaction rate existing from peak metamorphic conditions ($\sim 612^\circ \pm 17^\circ\text{C}$), at 29.7 ± 4.2 Ma, through early retrograde metamorphic conditions ($\sim 505^\circ \pm 15^\circ\text{C}$), at 16.5 ± 1.7 Ma, is therefore $1.3^{+1.1}_{-0.4} \times 10^{-7} \text{ g g}^{-1} \text{ year}^{-1}$.

Even without geochronological data, it is possible to obtain a limit on R from the value of Le . Using the mean value of Le (~ 0.7 m) and the equation for Le gives $R \approx (2 \text{ m}^{-2})D_{\text{Sr}}^*$. Taking plausible estimates for porosity [10^{-5} to 10^{-4} (2)], tortuosity [0.1 to 1.0 (22)], and K_{Sr} [1 to 10 (23)], and setting D_{Sr} to $0.6 \text{ m}^2 \text{ year}^{-1}$ for aqueous fluid diffusion (24) and ρ_s/ρ_f to 3, yields a D_{Sr}^* value between 2×10^{-5} and $2 \times 10^{-8} \text{ m}^2 \text{ year}^{-1}$. These represent maximum values, as the ITM may not be completely fluid-filled. The corresponding range in R is 4×10^{-5} to $4 \times 10^{-8} \text{ g g}^{-1} \text{ year}^{-1}$, which brackets the inferred value of $1.3 \times 10^{-7} \text{ g g}^{-1} \text{ year}^{-1}$ derived using the geochronological constraints.

Recent studies (25) suggest the possibility of episodic, short-lived (10^3 to 10^5 years duration) reactive-transport events characterized by high reactivity, which would be allowable by the constraint that $\langle R \rangle \approx 1.75$. However, knowledge of Le_{Sr} rules out the possibility that reaction rates were even transiently higher than $4 \times 10^{-5} \text{ g g}^{-1} \text{ year}^{-1}$, because D_{Sr}^* would need to be unreasonably high ($> 2 \times 10^{-5} \text{ m}^2 \text{ year}^{-1}$, see above). Furthermore, if R had been as high as $10^{-6} \text{ g g}^{-1} \text{ year}^{-1}$ for 2 million years (or $10^{-5} \text{ g g}^{-1} \text{ year}^{-1}$ for 200,000 years) at any time during metamorphism, the step in the solid profile at the contact would have been lost. Therefore, although the derived R applies directly only to the time between garnet growth and plagioclase closure, it is also unlikely that the prograde R could have been much higher than $10^{-7} \text{ g g}^{-1} \text{ year}^{-1}$.

Mineral chemistry data corroborate the inferences drawn from Sr isotopes about the scale and extent of reactive transport after garnet growth. Reaction coefficients (K_{eq}) were calculated, on the basis of mineral chemistry measurements, for 10 reactions (18). If local equilibrium had been maintained, the K_{eq} values for

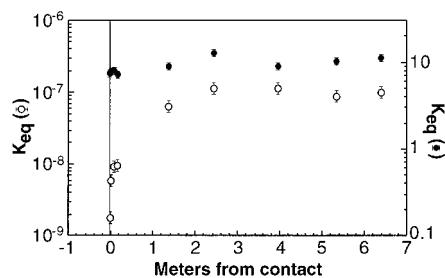


Fig. 3. Equilibrium constants (K_{eq}) calculated for two reactions: $3(\text{tremolite}) + 12(\text{anorthite}) = 4(\text{grossular}) + 2(\text{pyrope}) + 3(\text{tschermakite}) + 12(\text{quartz})$ (garnet-bearing, open circles) and $\text{tremolite} + 2(\text{albite}) + \text{tschermakite} = 2(\text{pargasite}) + 8(\text{quartz})$ (garnet-absent, solid circles).

each reaction should be the same throughout the outcrop, regardless of bulk composition. Garnet-absent reactions yield consistent K_{eq} values regardless of location (Fig. 3). Garnet-bearing reactions show a shift in K_{eq} within ~ 1 m of the contact, about the same scale as Le_{Sr} (~ 0.7 m). This is best explained by continued reaction between the matrix minerals (but not garnet porphyroblasts) accompanied by diffusive exchange of major elements [notably Ca and Na, given the shift in plagioclase composition toward the contact (18)] across the contact after garnet formation. These observations are contrary to the usual assumption that reactivity and transport are limited after peak metamorphism because of a lack of fluid (26).

The bulk solid-fluid exchange rate of $1.3^{+1.1}_{-0.4} \times 10^{-7} \text{ g g}^{-1} \text{ year}^{-1}$ is three to four orders of magnitude lower than surface area-normalized reaction rates \bar{R} (in grams per square centimeter per year) measured in laboratory studies (2, 3, 5). This raises questions about what controls natural reaction rates. Following transition state theory (2, 3, 5), $R = s\bar{R}$, where s is the reactive surface area in square centimeters per gram, and $\bar{R} = f(\Delta G, T)$, where ΔG is the free energy of reaction. Using $T = 600^\circ\text{C}$ and $|\Delta G| = 60 \text{ J mol}^{-1}$ —values representative of a small reaction overstep, and likely minima given the growing disequilibrium at our site—we can compare our bulk rate, $R = 1.3 \times 10^{-7} \text{ g g}^{-1} \text{ year}^{-1}$, to two laboratory-based values [$1.3 \times 10^{-4} \text{ g cm}^{-2} \text{ year}^{-1}$ (5) and $8.3 \times 10^{-4} \text{ g cm}^{-2} \text{ year}^{-1}$ (2) for an average solid of 35 g per mole of oxygen]. Reconciling the natural and lab-based data yields $s \leq 10^{-3}$ to $10^{-4} \text{ cm}^2 \text{ g}^{-1}$. Approximating minerals as spheres of radius 0.1 mm, representative of our samples, this implies that only 0.001% to 0.0001% of the mineral surface area is undergoing reaction, several orders of magnitude less than published estimates (3).

The inferred value of R approaches a rate that could be accounted for by solid-state diffusion alone. This suggests that diffusion may be an important exchange mechanism, and that the bulk solution-precipitation rate may be even lower than $10^{-7} \text{ g g}^{-1} \text{ year}^{-1}$. The inferred value of R is similar to deformation rates measured in the region (19) and raises the question of whether the two may be mechanically related.

The reaction time scale of $\sim 10^7$ years and evidence for major post-peak reactivity and transport suggests that mineral assemblages and chemistry may lag P-T-X conditions and that these effects must be accounted for in the sampling, analysis, and interpretation of metamorphic rocks. The garnet-whole rock disequilibrium and K_{eq} variations displayed within ~ 1 m of the contact will have negative effects on isotope dating and geothermobarometry, respectively, if not avoided. The R we infer is biased toward the reaction

rate of plagioclase, the dominant Sr-bearing mineral. The other minerals could have exchanged at a higher rate, as could have portions of zoned plagioclase. Microanalytical techniques have allowed additional information about crustal evolution to be gained from chemically zoned minerals; in this regard, slower bulk reaction rates can actually be favorable in that they confirm that rocks will have some useful memory of past conditions.

References and Notes

- See, for example, M. J. Bickle *et al.*, *J. Petrol.* **38**, 1489 (1997); L. O. Nicolaysen, *Ann. N.Y. Acad. Sci.* **2**, 198 (1961); F. S. Spear, *Metamorphic Phase Equilibria and Pressure-Temperature-Time Paths* (Mineralogical Society of America, Washington, DC, 1993).
- J. V. Walther and B. J. Wood, in *Fluid-Rock Interactions During Metamorphism*, J. V. Walther and B. J. Wood, Eds. (Springer-Verlag, New York, 1986), pp. 195–211.
- H. C. Helgeson, W. M. Murphy, P. Aagaard, *Geochim. Cosmochim. Acta* **48**, 2405 (1984).
- B. R. Hacker, S. H. Kirby, S. R. Bohlen, *Science* **258**, 110 (1992); C. Jove and B. R. Hacker, *Am. Mineral.* **82**, 781 (1997).
- J. A. Schramke, D. M. Kerrick, A. C. Lasaga, *Am. J. Sci.* **287**, 517 (1987).
- A. D. L. Skelton, M. J. Bickle, C. M. Graham, *Earth Planet. Sci. Lett.* **146**, 527 (1997); J. J. Ague, *Contrib. Mineral. Petrol.* **132**, 180 (1998); A. C. Lasaga and D. M. Rye, *Am. J. Sci.* **293**, 361 (1993); H. Eppel and R. Abart, *Am. J. Sci.* **297**, 707 (1997).
- D. J. DePaolo and S. R. Getty, *Geochim. Cosmochim. Acta* **60**, 3933 (1996).
- The ITM may be a fluid, "dry" grain boundaries, or some combination. The nature of the ITM is not prescribed by the model.
- The overall chemical affinity is a measure of the sum, over all independent reactions, of the free energy departure from equilibrium. See (3) for discussion.
- Transport could also occur by diffusion through solid mineral grains, or by an advecting fluid. Numerous studies [J. M. Ferry, *Am. J. Sci.* **294**, 905 (1994); M. J. Kohn and J. W. Valley, *Geochim. Cosmochim. Acta* **58**, 5551 (1994); (16)] have shown that cross-contact advection is limited, and where present can usually be recognized. There is no evidence of cross-contact advection at the contact under study. Solid-state diffusion is much slower than grain-boundary or fluid-mediated diffusion.
- R , in units of grams of solid reacted per gram of solid per year, is the rate at which the bulk solid reacts and exchanges with the ITM. It is expressed as $R = \sum R_i M_i (C_i/C_{\text{bulk}})$: the sum of the reaction rates, R_i , for all minerals, weighted by their Sr concentration (C_i/C_{bulk}) and mode (M_i). Although the model incorporates dissolution-precipitation as the sole mechanism for reaction, the R we measure includes the effects of all operating exchange mechanisms. If solid-state diffusion is an important exchange mechanism, the deduced value of R will be higher than the actual bulk rate of dissolution-precipitation.
- Le is the length scale over which the changing fluid remains in disequilibrium with the solid. Perfect local equilibrium corresponds to $Le = 0$. For a full discussion, see O. M. Phillips, *Flow and Reactions in Permeable Rocks* (Cambridge Univ. Press, New York, 1991), pp. 96–100.
- Equations assume constant porosity and Sr concentration in time and space, as well as spatially constant D^* and R .
- $\lambda = 1.42 \times 10^{-11} \text{ year}^{-1}$ is the decay constant of ^{87}Rb . The r_{ps} profile (r_{ps} is the $^{87}\text{Rb}/^{86}\text{Sr}$ ratio) is set to measured values and kept constant in time.
- When garnets grow during metamorphism, they take on the local fluid (ITM) composition and are resistant to further exchange because of their exceedingly slow intracrystalline diffusion. This property of garnet has been exploited to determine metamorphic chemical, P-T, and deformation histories [e.g., F. S. Spear

- and J. Selverstone, *Contrib. Mineral. Petrol.* **83**, 348 (1982); (19)].
16. C. R. Vyhnal and C. P. Chamberlain, *Am. J. Sci.* **296**, 394 (1996). At our field locality, there probably was diagenetic exchange that caused the $^{87}\text{Sr}/^{86}\text{Sr}$ of the amphibolite protolith to be increased from about 0.703 (based on the Nd isotope data) to about 0.705 or 0.706. The pelite value may also have been affected.
 17. The Lebendun Nappe here contains three horizons of garnet amphibolite (8 to 15 m thick) interlayered with pelite. The "pelite" grades from a quartz-rich (86% SiO_2) psammite at the contact to a more typical pelite (75% SiO_2) within ~10 cm. The amphibolite contains biotite, which decreases in mode away from the contact, and garnet porphy-

- roblasts up to 5 mm in diameter. At the contact, garnets are more sparse and rarely exceed 500 μm in diameter. Pelitic garnets continue to decrease in diameter and mode away from the contact, <200 μm near the contact and reaching zero after several meters.
18. See www.sciencemag.org/feature/data/1049980.shtml for supplementary raw data and analytical methods.
 19. D. Vance and R. K. O'Nions, *Earth Planet. Sci. Lett.* **114**, 113 (1992).
 20. This is because $K_{\text{Nd}} \gg K_{\text{Sr}}$ such that D_{Nd}^* is very small.
 21. N. S. Mancktelow, *Tectonophysics* **215**, 295 (1992).
 22. J. B. Brady, *Am. J. Sci.* **283A**, 181 (1983).
 23. A. R. Kotelnikov, I. V. Chernysheva, M. S. Parmuzina, *Geochem. Int.* **36**, 846 (1998).

24. E. H. Oelkers and H. C. Helgeson, *Geochim. Cosmochim. Acta* **52**, 63 (1988).
25. C. M. Graham, J. W. Valley, J. M. Eiler, H. Wada, *Contrib. Mineral. Petrol.* **132**, 371 (1998); J. L. M. van Haren, J. J. Ague, D. M. Rye, *Geochim. Cosmochim. Acta* **60**, 3487 (1996); E. D. Young and D. Rumble, *Geochim. Cosmochim. Acta* **57**, 2585 (1993).
26. J. V. Walther, *J. Geol.* **102**, 559 (1994).
27. We thank J. J. Ague, J. G. Bryce, and several anonymous reviewers for valuable reviews and discussions, and J. Selverstone and T. Wawrzyniec for assisting in field site selection. Supported by NSF grant EAR-9805218 (D.J.D.) and a Berkeley Geochronology Center Fellowship (E.F.B.).

11 February 2000; accepted 21 March 2000

Spatial Patterns in the Distribution of Tropical Tree Species

Richard Condit,^{1*} Peter S. Ashton,² Patrick Baker,³ Sarayudh Bunyavejchewin,⁴ Savithri Gunatilleke,⁵ Nimal Gunatilleke,⁵ Stephen P. Hubbell,⁶ Robin B. Foster,⁷ Akira Itoh,⁸ James V. LaFrankie,⁹ Hua Seng Lee,¹⁰ Elizabeth Losos,¹ N. Manokaran,¹¹ R. Sukumar,¹² Takuo Yamakura⁸

Fully mapped tree census plots of large area, 25 to 52 hectares, have now been completed at six different sites in tropical forests, including dry deciduous to wet evergreen forest on two continents. One of the main goals of these plots has been to evaluate spatial patterns in tropical tree populations. Here the degree of aggregation in the distribution of 1768 tree species is examined based on the average density of conspecific trees in circular neighborhoods around each tree. When all individuals larger than 1 centimeter in stem diameter were included, nearly every species was more aggregated than a random distribution. Considering only larger trees (≥ 10 centimeters in diameter), the pattern persisted, with most species being more aggregated than random. Rare species were more aggregated than common species. All six forests were very similar in all the particulars of these results.

The spatial dispersion of individuals in a species is central in ecological theory (1, 2). Patchiness, or the degree to which individuals are aggregated or dispersed, is crucial to how a species uses resources, to how it is used as a resource, and to its reproductive biology. Spatial patterns have been a particularly important theme in tropical ecology, because high diversity in the tropics begets low densities. Since Wallace (3) noted how difficult it was to find two individuals of the same species, the hyperdispersion of tropical trees has focused much of theoretical tropical ecology.

In 1979, Hubbell (4) published a large study of dispersion of trees in a dry forest in Costa Rica. His results were contrary to Wallace's long-prevailing wisdom and the Janzen–Connell prediction (5, 6) that wide dispersion is a defense against predators. Most species were aggregated, so that near neighborhoods of a tree had a higher than average density of conspecifics. Since that study,

though, contradictory results have appeared, particularly from Lieberman and Lieberman (7), who found that most species in a wet forest in Costa Rica, as well as from a literature survey, were not aggregated.

Over the past two decades, we have been assembling a long-term, large-scale, global research effort on spatial patterns and dynamics of tropical forests (8, 9). An international team has now fully censused six plots in five tropical countries, mapping and identifying every individual of ≥ 1 cm in stem diameter over 25 to 52 ha at each plot (Table 1). The large plot size is necessary to encompass substantial populations of most tree species in the community. Major goals of this effort have been to examine Janzen–Connell effects, density dependence, and the spacing pattern of individual species.

The six sites represent a wide variety of tropical forests (Table 1). At one extreme, the two plots in Malaysia are in tall, evergreen forest; have no regular dry season; and include

over 800 tree and treelet species each. The Sinharaja forest is also very wet and evergreen, but its island setting reduces species diversity. The site in India is in dry forest with a fairly open canopy, grassy understory, and just 70 species; the Thai site is also dry and low in diversity. The single site in Central America is moist forest, structurally quite like the Malaysian sites, but intermediate in climate and diversity. The forests also cover a wide taxonomic range. Four of the Asian sites are dominated by the family Dipterocarpaceae, but few species are shared among them. The Indian and American sites are distinct taxonomically; they are not dominated by a single family and have few (India) or no (Panama) dipterocarps.

We evaluate spatial patterning by examining neighborhoods around individual trees. For each individual, we tallied the number of conspecifics between x and $x + \Delta x$ meters for all $x + \Delta x$ inside the plot. We also calculated the area inside the plot of each of these annuli. The number of neighbors N_x and the area A_x in each annulus at distance x were then summed over all individuals of a given species. $D_x = \Sigma N_x / \Sigma A_x$ gives the density of neighboring conspecifics as a function of distance from the average individual. This is a biologically meaningful measure of clumping, because it evaluates the conspecific population density in the neighborhood of

¹Center for Tropical Forest Science, Smithsonian Tropical Research Institute, Unit 0948, APO AA 34002–0948, USA. ²Center for Tropical Forest Science, Harvard Institute for International Development and Harvard University, Cambridge, MA 02138, USA. ³Silviculture Laboratory, College of Forest Resources, University of Washington, Seattle, WA 98195–2100, USA. ⁴Royal Thai Forest Department, Chatuchak, Bangkok 10900, Thailand. ⁵Department of Botany, University of Peradeniya, Peradeniya, Sri Lanka. ⁶Center for Tropical Forest Science, University of Georgia, Athens, GA 30602, USA. ⁷Center for Tropical Forest Science, Field Museum of Natural History, Chicago, IL 60605–2496, USA. ⁸Osaka City University, Osaka 558-8585, Japan. ⁹Center for Tropical Forest Science, National Institute of Education, Singapore 1025. ¹⁰Sarawak Forest Department, Kuching, Sarawak 93660, Malaysia. ¹¹Forest Research Institute of Malaysia, Kepong 52109, Kuala Lumpur, Malaysia. ¹²Indian Institute of Science, Bangalore 560012, India.

*To whom correspondence should be addressed. E-mail: cfts@tivoli.si.edu